

## Biophysical Characterization of A $\beta$ 42 C-Terminal Fragments: Inhibitors of A $\beta$ 42 Neurotoxicity<sup>†</sup>

Huiyuan Li,<sup>‡</sup> Bernhard H. Monien,<sup>‡,§</sup> Erica A. Fradinger,<sup>‡,||</sup> Brigita Urbanc,<sup>⊥</sup> and Gal Bitan<sup>\*,‡,§,⊥,Δ</sup>

<sup>‡</sup>Department of Neurology, David Geffen School of Medicine, <sup>#</sup>Brain Research Institute, and <sup>Δ</sup>Molecular Biology Institute, University of California, Los Angeles, 635 Charles E. Young Drive, Los Angeles, California 90095, and <sup>⊥</sup>Physics Department, Drexel University, 3141 Chestnut Street, Philadelphia, Pennsylvania 19104 <sup>§</sup>Current address: Deutsches Institut für Ernährungsforschung Potsdam-Rehbrücke, Abteilung Ernährungstoxikologie, Arthur-Scheunert-Allee 114-116, 14558 Nuthetal, Germany <sup>||</sup>Current address: Department of Biology, Whittier College, 13406 E. Philadelphia St., Whittier, CA 90608

Received December 3, 2009; Revised Manuscript Received January 1, 2010

**ABSTRACT:** A key event in Alzheimer's disease (AD) is age-dependent, brain accumulation of amyloid  $\beta$ -protein (A $\beta$ ) leading to A $\beta$  self-association into neurotoxic oligomers. Previously, we showed that A $\beta$  oligomerization and neurotoxicity could be inhibited by C-terminal fragments (CTFs) of A $\beta$ 42. Because these CTFs are highly hydrophobic, we asked if they themselves aggregated and, if so, what parameters regulated their aggregation. To answer these questions, we investigated the dependence of CTF aqueous solubility, aggregation kinetics, and morphology on peptide length and sequence and the correlation between these characteristics and inhibition of A $\beta$ 42-induced toxicity. We found that CTFs up to 8 residues long were soluble at concentrations > 100  $\mu$ M and had a low propensity to aggregate. Longer CTFs were soluble at  $\sim$ 1–80  $\mu$ M, and most, but not all, readily formed  $\beta$ -sheet-rich fibrils. Comparison to A $\beta$ 40-derived CTFs showed that the C-terminal dipeptide I41-A42 strongly promoted aggregation. Aggregation propensity correlated with the previously reported tendency to form  $\beta$ -hairpin conformation but not with inhibition of A $\beta$ 42-induced neurotoxicity. The data enhance our understanding of the physical characteristics that affect CTF activity and advance our ability to design, synthesize, and test future generations of inhibitors.

A key event in Alzheimer's disease (AD)<sup>1</sup> etiology is assembly of amyloid  $\beta$ -protein (A $\beta$ ) into neurotoxic oligomers (1). A $\beta$  oligomers induce severe neuronal injury and likely are the primary neurotoxins acting in AD (2–6). Two predominant forms of A $\beta$  comprising 40 (A $\beta$ 40) or 42 (A $\beta$ 42) amino acid residues are produced *in vivo*. The difference between A $\beta$ 40 and A $\beta$ 42 is the absence or presence of the C-terminal residues I41 and A42, respectively. Though this is a small structural difference, it has strong implications on the biophysical and biological behaviors of the two A $\beta$  alloforms. A $\beta$ 42 has been shown to be more neurotoxic (7), form higher order oligomers, and follow a different oligomerization pathway compared to A $\beta$ 40 (8, 9). These observations correlate with structural stabilization of the C-terminus of A $\beta$ 42 by the I41-A42 dipeptide (8, 10, 11). Studies using discrete molecular dynamics have suggested that a turn centered at G37-G38 rigidifies the C-terminus in A $\beta$ 42 but not A $\beta$ 40 (12, 13). In agreement with these results, using replica-exchange molecular dynamics with an all-atom protein model,

Yang et al. also found that in A $\beta$ 42 the sequences spanning residues 28–37 and 39–42 are connected by a turn, which was stabilized by multiple hydrophobic interactions involving I41 and A42 (14). Multiple solution-state nuclear magnetic resonance (NMR) studies of aqueous A $\beta$ 40 and A $\beta$ 42 (15–18) support the notion that the C-terminus of A $\beta$ 42 is more rigid than that of A $\beta$ 40.

In view of the critical role of the C-terminal region of A $\beta$ 42 in self-assembly, we hypothesized that peptides derived from this region might disrupt A $\beta$ 42 self-assembly and therefore inhibit A $\beta$ 42 toxicity. To test this hypothesis, we prepared a series of C-terminal fragments (CTFs) of A $\beta$ 42, [A $\beta$ (x–42), x = 28–39] (19) (Table 1) and evaluated their efficacy as inhibitors of A $\beta$ 42-induced neurotoxicity (20). All CTFs except A $\beta$ (28–42) showed significant inhibition of A $\beta$ 42-induced toxicity. Of the 12 CTFs tested, A $\beta$ (30–42), A $\beta$ (31–42), and A $\beta$ (39–42) were the strongest inhibitors (20). Interestingly, inhibition of toxicity did not correlate with peptide length and had a complex relationship with peptide sequence. These findings raised questions regarding the biophysical properties of CTFs themselves: how the sequence relates to the biophysical properties of each peptide and what structural/biophysical features contribute to inhibition of A $\beta$ 42-induced toxicity. Answering these questions is critical for designing future generations of CTF-based peptidomimetic inhibitors of A $\beta$  assembly and toxicity.

Here, we characterized the aqueous solubility of the CTFs and their tendency to aggregate into fibrils and form  $\beta$ -sheet and correlated these characteristics with the previously characterized inhibition of A $\beta$ 42-induced toxicity. To gain further insight into

<sup>†</sup>The work was supported by Grants AG027818 from the NIH/NIA and 2005/2E from the Larry L. Hillblom Foundation.

\*To whom correspondence should be addressed at the Department of Neurology, David Geffen School of Medicine, University of California at Los Angeles. E-mail: gbitan@mednet.ucla.edu. Tel: 310-206-2082. Fax: 310-206-1700.

Abbreviations: AAA, amino acid analysis; A $\beta$ , amyloid  $\beta$ -protein; AD, Alzheimer's disease; CD, circular dichroism spectroscopy; CTF, C-terminal fragment; DLS, dynamic light scattering; EM, electron microscopy; IM-MS, ion-mobility mass spectrometry; MD, molecular dynamics; MTT, 3-(4,5-dimethylthiazol-2-yl)-2,5-diphenyltetrazolium bromide; NMR, nuclear magnetic resonance.

Table 1: Biological and Biophysical Characteristics of A $\beta$ 42 CTFs and Control Peptides

peptide	sequence	cell viability <sup>a</sup> (%)	max solubility <sup>b</sup> ( $\mu$ M)	aggregation rate <sup>c</sup> (nm/h)	$\beta$ -sheet formation, $T_{50}$ <sup>d</sup> (h)	$\beta$ -hairpin <sup>e</sup> (%)	coil-turn <sup>e</sup> (%)
A $\beta$ (39–42)	VVIA	89 $\pm$ 5***	140 $\pm$ 30	–	–	–	–
A $\beta$ (38–42)	GVVIA	83 $\pm$ 3***	156 $\pm$ 33	–	–	–	–
A $\beta$ (37–42)	GGVVIA	73 $\pm$ 2***	143 $\pm$ 27	–	–	–	–
A $\beta$ (36–42)	VGGVVIA	80 $\pm$ 3***	134 $\pm$ 19	–	–	–	–
A $\beta$ (35–42)	MVGGVVIA	82 $\pm$ 4***	149 $\pm$ 33	–	–	–	–
A $\beta$ (34–42)	LMVGGVVIA	76 $\pm$ 3***	132 $\pm$ 29	–	–	–	–
A $\beta$ (33–42)	GLMVGGVVIA	81 $\pm$ 3***	134 $\pm$ 37	1.8 $\pm$ 0.2	25 $\pm$ 3	–	–
A $\beta$ (32–42)	IGLMVGGVVIA	79 $\pm$ 2***	54 $\pm$ 24	–	–	–	–
A $\beta$ (31–42)	IIGLMVGGVVIA	105 $\pm$ 5***	62 $\pm$ 17	1.0 $\pm$ 0.2	36 $\pm$ 4	25	29
A $\beta$ (30–42)	AIIGLMVGGVVIA	97 $\pm$ 4***	11 $\pm$ 3	8.8 $\pm$ 3.4	6.6 $\pm$ 0.3	42	16
A $\beta$ (29–42)	GAIIGLMVGGVVIA	72 $\pm$ 3**	22 $\pm$ 9	6.6 $\pm$ 3.3	4.1 $\pm$ 0.1	43	4
A $\beta$ (28–42)	KGAIIGLMVGGVVIA	–	~1	–	–	–	–
A $\beta$ (34–40)	LMVGGVV	66 $\pm$ 2	169 $\pm$ 13	–	–	–	–
A $\beta$ (30–40)	AIIGLMVGGVV	98 $\pm$ 7***	196 $\pm$ 1	0.3 $\pm$ 0.1	–	4	28
A $\beta$ (21–30)	AEDVGSNKGA	63 $\pm$ 7	129 $\pm$ 5	–	–	–	–

<sup>a</sup>Cell viability (mean  $\pm$  SEM) was calculated from at least three independent experiments ( $n \geq 18$ ). Statistical significance was calculated compared with A $\beta$ 42 alone using student's *t*-test. \*\*\*,  $p < 0.001$ ; \*\*,  $p < 0.01$ . <sup>b</sup>Maximal average solubility (mean  $\pm$  SEM) was measured by AAA in four to seven measurements. The cell viability and solubility data of CTFs reported previously (20) are shown here for comparison. <sup>c</sup>Particle growth rates (mean  $\pm$  SEM) were calculated from three independent measurements. <sup>d</sup> $T_{50}$  values were determined by sigmoidal regression using the function  $f(x) = y_0 + a/(1 + e^{x_0 - x/b})$  (Figure 2C). <sup>e</sup>The percentage of CTF superclusters obtained by IM-MS and MD simulations in water at 300 K (44). “–” means no data available for this peptide. Blank cells mean data not obtained for this peptide.

the specific interactions that affect CTF properties, in addition to the original A $\beta$ 42 CTF series, we included two A $\beta$ 40-derived CTFs, A $\beta$ (34–40) and A $\beta$ (30–40), to evaluate the importance of the C-terminal I41–A42 dipeptide at the C-terminus of A $\beta$ 42, and the sequence A $\beta$ (21–30), which contains the putative folding nucleus of both A $\beta$ 40 and A $\beta$ 42 (11). The sequences of additional peptides are shown in Table 1. We present a systematic study of the aggregation properties of these peptides and discuss relationships among sequence, biophysical properties, and inhibition of A $\beta$ 42 toxicity.

## MATERIALS AND METHODS

**Peptide Preparation.** A $\beta$ 42 was synthesized by solid-phase techniques (21) using 9-fluorenylmethoxycarbonyl chemistry, as described previously (22), purified by high-performance liquid chromatography, and analyzed by mass spectrometry and amino acid analysis (AAA). A $\beta$ (30–40), A $\beta$ (34–40), and A $\beta$ (21–30) were prepared using the same method. A $\beta$ 42 CTFs were prepared and characterized as described previously (19).

**Toxicity Inhibition Assay.** Inhibition of A $\beta$ 42-induced toxicity was performed as described previously (20). Briefly, PC-12 cells were used 48 h after differentiation. Solutions of A $\beta$ 42 and each peptide at a 1:10 concentration ratio, respectively, were incubated with the cells for 15 h. Cell viability was determined by the 3-(4,5-dimethylthiazol-2-yl)-2,5-diphenyltetrazolium bromide (MTT) assay using the CellTiter 96 kit (Promega, Madison, WI). Negative controls included DMSO at the same concentration as in the peptide solutions and media alone. A positive control was 1  $\mu$ M staurosporine for full kill, which was used to represent a 100% reduction in cell viability, based on which the percentage viability of all of the experimental conditions was calculated. At least three independent experiments with six replicates ( $n \geq 18$ ) were carried out, and the results were averaged and presented as mean  $\pm$  SEM.

**Solubility.** Peptide solutions or suspensions were prepared at 200  $\mu$ M nominal concentration by dissolution at 2 mM in 60 mM NaOH and dilution with 10 mM sodium phosphate, pH 7.4, to the final nominal concentration. The solution was

sonicated for 1 min and then filtered through an Anotop 10 syringe filter with 20 nm pore size (Whatman, Florham Park, NJ). Parallel recordings of CD and DLS data started immediately following filtration. Four to seven replicates were measured for each peptide. The actual peptide concentrations were determined by AAA, and the results were presented as mean  $\pm$  SEM.

**Dynamic Light Scattering.** Peptide solutions were measured using an in-house-built system with a He–Ne laser, model 127 (wavelength 633 nm, power 60 mW; Spectra Physics Lasers, Mountain View, CA). Light scattered at 90° was collected using image-transfer optics and detected by an avalanche photodiode built into a 256-channel PD2000DLS correlator (Precision Detectors, Bellingham, MA). The size distribution of scattering particles was reconstructed from the scattered light correlation function using PrecisionDeconvolve software (Precision Detectors) based on the regularization method by Tikhonov and Arsenin (23). The data are an average of three independent experiments.

**Circular Dichroism Spectroscopy.** Far-UV CD spectra were recorded using a J-810 spectropolarimeter (Jasco, Easton, MD) with a thermostable sample cell (23 °C) using cuvettes with 1 mm path length. Twenty measurements were collected between 190 and 260 nm with 1 s response time, 20 nm/min scan speed, 0.2 nm resolution, and 2 nm bandwidth and averaged after background subtraction. Measurements were taken every 24 h for 4 days for A $\beta$ (33–42) through A $\beta$ (39–42) and in shorter time intervals for longer CTFs. The data are representative of three independent experiments. All CD data were converted from CD signal (millidegrees) into mean residue molar ellipticity ( $\text{deg} \cdot \text{cm}^2 \cdot \text{dmol}^{-1}$ ) using the equation  $[\theta] = (\theta \times 10^{-1})/l \cdot c^{-1}$ , where  $l$  is the path length in centimeters and  $c$  is the molar concentration. Secondary structure content initially was calculated using the deconvolution programs Selcon3 (24), ContinLL (25), and CDSstr (26) within the CDpro (2004) software package. ContinLL consistently generated fits with the lowest root-mean-square deviations among these three programs and therefore was chosen for deconvolution of all CD spectra.

**Electron Microscopy.** Eight microliter aliquots of peptide solutions were spotted on glow-discharged, carbon-coated Formvar grids (Electron Microscopy Science, Hatfield, PA). Samples of A $\beta$ (37–42) through A $\beta$ (39–42) were incubated for 30 min, A $\beta$ (32–42) through A $\beta$ (36–42) for 15–20 min, A $\beta$ (30–40), A $\beta$ (34–40), and A $\beta$ (21–30) for 10 min, and A $\beta$ (28–42) through A $\beta$ (31–42) for 60–90 min. The solutions were wicked gently with filter paper. The samples were then fixed with 5  $\mu$ L of 2.5% glutaraldehyde for 20 min and stained with 5  $\mu$ L of 2% uranyl acetate for 30 min (A $\beta$ (28–42) through A $\beta$ (31–42)) or 1% uranyl acetate for 10 min (A $\beta$ (32–42) through A $\beta$ (39–42), A $\beta$ (30–40), A $\beta$ (34–40), and A $\beta$ (21–30)). After cautious removal of staining solutions with filter paper, the grids were air-dried. Three to six replicates of each peptide were analyzed using a CX 100 transmission electron microscope (JEOL, Peabody, MA). The diameter and length of each peptide were analyzed using ImageJ (available at <http://rsbweb.nih.gov/ij/>). Ten separate measurements were averaged and the data reported as mean  $\pm$  SEM.

## RESULTS

**Inhibition of A $\beta$ 42-Induced Toxicity.** Previously, a cell-viability screen showed that all CTFs of A $\beta$ 42, except A $\beta$ (28–42), which was highly toxic itself, inhibited A $\beta$ 42-induced toxicity (20). Here, we characterized the two A $\beta$ 40 CTFs and A $\beta$ (21–30) by the same viability assay using the MTT assay (27, 28) in differentiated PC-12 cells (29, 30) with 5  $\mu$ M A $\beta$ 42 and a 10-fold excess of each peptide. A $\beta$ 42 alone caused a robust ( $\approx$ 40%) reduction in cell viability. A $\beta$ (30–40) showed strong inhibitory effect of A $\beta$ 42-induced toxicity, similar to A $\beta$ (39–42) and A $\beta$ (30–42), whereas A $\beta$ (34–40) and A $\beta$ (21–30) were inactive. The cell viability of CTFs and control peptides is shown in Table 1.

**Peptide Solubility.** CTFs are highly hydrophobic peptides (19) and therefore are expected to be poorly soluble and aggregate in aqueous solutions. To estimate peptide solubility, we used a simple filtration assay. Lyophilized peptides were dissolved or suspended in 10 mM sodium phosphate at 200  $\mu$ M nominal concentration (see Materials and Methods), sonicated for 1 min, and filtered through a 20 nm pore-size filter (alumina-based polar membrane) to remove insoluble material. Following this treatment, the actual concentrations were determined by AAA and are shown in Table 1.

CTFs up to 10 amino acids long were found to be soluble between  $\sim$ 100 and 200  $\mu$ M. Longer peptides were soluble between  $\sim$ 10 and 80  $\mu$ M except for the longest CTF, A $\beta$ (28–42), which was found to have the lowest solubility ( $\sim$ 1  $\mu$ M). Both A $\beta$ 40 CTFs had higher solubility in this assay than any of the A $\beta$ 42 CTFs. The solubility found for A $\beta$ (21–30) ( $\sim$ 130  $\mu$ M) was surprisingly lower than expected considering the hydrophilic nature of this peptide and previous solution-state NMR studies done at millimolar concentrations in ammonium acetate, pH 6.0, at 10  $^{\circ}$ C (11, 31, 32). We note that an underlying assumption in using the filtration assay was that the degree of nonspecific adsorption of the peptides to the filter membrane would be independent of the sequence. This assumption likely is reasonable for the CTFs, which are all highly hydrophobic. However, the unexpectedly low concentration found for A $\beta$ (21–30) following filtration presumably reflects strong adsorption of this highly polar peptide on the polar, alumina-based filter membrane, rather than actual solubility.

**Peptide Aggregation.** The limited solubility of CTFs, particularly those longer than 10 residues, was expected, taking into

account that they originated from the hydrophobic C-terminus of A $\beta$ 42. To elucidate further the behavior of these peptides, we asked whether their low solubility was a result of clumping together to form amorphous aggregates or reflected aggregation into amyloid fibrils. Amyloid fibrils are noncrystalline but have a high degree of order, reflected in a cross- $\beta$ -structure, in which  $\beta$ -strands are arranged perpendicular to the fibril axis (33, 34). To answer this question, we studied time-dependent particle growth, conformational change, and morphology of the peptides using dynamic light scattering (DLS), circular dichroism (CD) spectroscopy, and electron microscopy (EM), respectively.

Ideally, the kinetics of aggregation and conformational transition would have been studied with all peptides at the same concentration. However, this was not feasible because the solubility of the CTFs varied over 2 orders of magnitude. If all CTFs had been diluted to the concentration of the least soluble peptide ( $<$  10  $\mu$ M), observation of aggregation, conformational transitions, or morphological changes for the more soluble peptides would have necessitated to conduct experiments for weeks or even months. Instead, we studied the peptides at their maximal concentration following filtration through 20 nm pore-size filters as described above. In a limited number of cases, certain peptides were diluted to allow comparing aggregation rates of different peptides at similar concentrations.

To study particle size growth over time, we used DLS, a common method for studying protein aggregation noninvasively (35–37). When evaluating the data obtained here, it is important to keep in mind that because the peptides could not be studied at the same concentration, the interpretation of the data is qualitative and not quantitative. We found that most of the A $\beta$ 42 CTFs, including A $\beta$ (32–42) ( $\sim$ 55  $\mu$ M), A $\beta$ (35–42) through A $\beta$ (39–42) ( $>$  100  $\mu$ M), and also A $\beta$ (34–40) ( $\sim$ 170  $\mu$ M) and A $\beta$ (21–30) ( $\sim$ 130  $\mu$ M), did not show appreciable particle growth up to 96 h. In addition, the solubility of A $\beta$ (28–42) was too low to allow reliable measurement, and the aggregation of A $\beta$ (34–42) ( $\sim$ 130  $\mu$ M) was slow, and the spectra had low signal-to-noise ratio that precluded reliable calculation of aggregation rate. Particle growth was observed for A $\beta$ ( $x$ –42) CTFs with  $x$  = 29, 30, 31, and 33 and for A $\beta$ (30–40). The change in hydrodynamic radius ( $R_H$ ) of these CTFs over 96 h is shown in Figure 1A, and the average particle growth rate ( $dR_H/dt$ ) is given in Figure 1B and Table 1. The general trend among those four A $\beta$ 42 CTFs was faster aggregation with longer sequence, but the correlation between length and aggregation kinetics was not linear. A $\beta$ (29–42) and A $\beta$ (30–42) aggregated substantially faster than A $\beta$ (31–42) and A $\beta$ (33–42) even though they were measured at substantially lower concentrations. A $\beta$ (30–40) aggregated more slowly than the four A $\beta$ 42 CTFs despite similar length, demonstrating the strong contribution of the I41-A42 dipeptide to promoting aggregation.

It is noteworthy that immediately following filtration through a 20 nm pore-size filter ( $t$  = 0), particles of  $R_H$  = 40–100 nm were observed for the A $\beta$ 42 CTFs shown in Figure 1A, indicating that some rapid self-association occurred. Nevertheless, the total intensity of scattering was low, suggesting that most of the peptide existed in a disassembled state or as small oligomers. This suggests that relatively few 40–100 nm particles formed rapidly between the end of the filtration and the beginning of DLS measurement (1–2 min). Such particles also may have extended rather than globular shapes, which would result in a large measured  $R_H$ .

**Secondary Structure.** We used CD spectroscopy to investigate the correlation between aggregation and  $\beta$ -sheet formation.

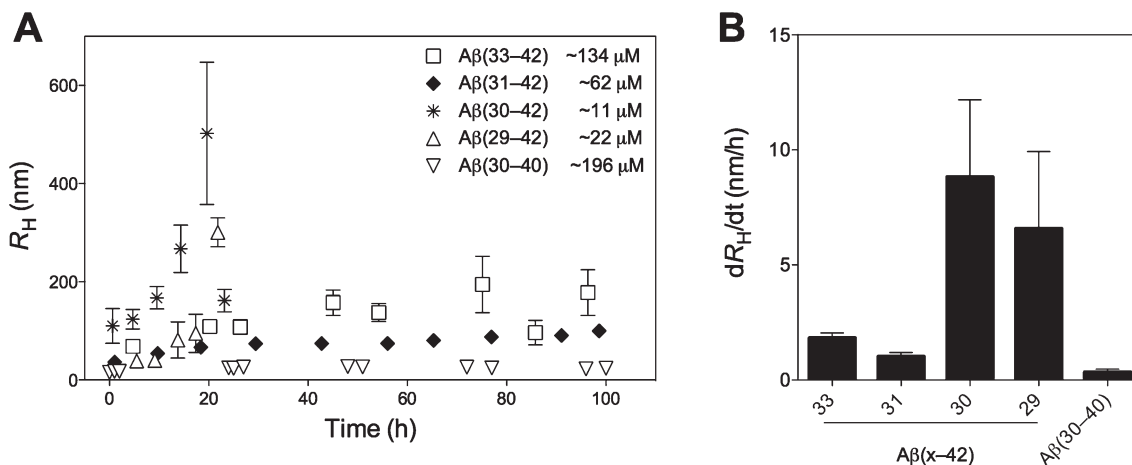


FIGURE 1: Particle growth rate. (A) Time course of average  $R_H$  was calculated from whole particle size distributions in solutions of  $A\beta(29-42)$ ,  $A\beta(30-42)$ ,  $A\beta(31-42)$ ,  $A\beta(33-42)$ , or  $A\beta(30-40)$  at the concentrations indicated. Each data point represents mean  $\pm$  SEM calculated from the average  $R_H$  of eight consecutive DLS measurements during 45–60 min. Aggregation of  $A\beta(29-42)$  and  $A\beta(30-42)$  was followed until the upper limit of detection was reached. (B) Average aggregation rates of  $A\beta(29-42)$ ,  $A\beta(30-42)$ ,  $A\beta(31-42)$ ,  $A\beta(33-42)$ , and  $A\beta(30-40)$ . The data represent mean  $\pm$  SEM of three independent experiments.

CD spectra of each peptide were recorded over 96 h. In general, the data observed were in agreement with the DLS results. The initial spectra of all peptides showed a high proportion of unordered structure. The spectra of  $A\beta(32-42)$ ,  $A\beta(35-42)$  through  $A\beta(39-42)$ ,  $A\beta(34-40)$ , and  $A\beta(21-30)$  did not change during the experiment. Figure 2A shows characteristic CD spectra of  $\sim 150 \mu\text{M}$   $A\beta(38-42)$  as an example. Other peptides showed a time-dependent spectral change from a minimum at 197 nm to a maximum at 198 nm with simultaneous development of a minimum at 218 nm indicating transformation from unordered conformation to a  $\beta$ -sheet-rich structure. Figure 2B shows characteristic CD spectra of  $\sim 60 \mu\text{M}$   $A\beta(31-42)$  as an example. Similar changes in the spectra, albeit at different rates, were observed for  $A\beta 42$  CTFs longer than  $A\beta(35-42)$  except  $A\beta(32-42)$  and for  $A\beta(30-40)$ . In all cases, an isodichroic point was observed at 212 nm, indicating a one-step transition from unstructured to  $\beta$ -sheet-rich conformation.

To quantify the rate of secondary structure transformation, the spectra were deconvoluted using the program ContinLL (25). A representative time-course of  $\beta$ -sheet formation is shown in Figure 2C. The time in which half-maximal  $\beta$ -sheet conformation formed ( $T_{50}$ , Table 1) was calculated to facilitate quantitative comparison with solubility and DLS data.  $A\beta(34-42)$  and  $A\beta(30-40)$  showed a small increase in  $\beta$ -sheet content at  $\sim 170$  and  $\sim 195 \mu\text{M}$ , respectively, during the time of measurement.  $A\beta(33-42)$  did not show conformational conversion at  $\sim 50 \mu\text{M}$ , whereas at  $\sim 130 \mu\text{M}$  it converted to  $\beta$ -sheet at a rate similar to that of  $A\beta(31-42)$  at  $\sim 60 \mu\text{M}$ .  $A\beta(29-42)$  at  $\sim 20 \mu\text{M}$  and  $A\beta(30-42)$  at  $\sim 10 \mu\text{M}$  converted to  $\beta$ -sheet within several hours (Figure 2C). Consistent with the DLS results,  $A\beta(32-42)$  appeared to be an outlier. At  $\sim 55 \mu\text{M}$ ,  $A\beta(32-42)$  showed no conformational change up to 96 h, suggesting that, in contrast to other CTFs, this CTF formed unordered, rather than fibrillar aggregates.

**Morphology.** To determine the morphology of peptide aggregates, aliquots of each peptide solution were examined by EM directly after dissolution (day 1) and following incubation for 7 days (Figure 3).

Electron micrographs of  $A\beta(35-42)$  through  $A\beta(39-42)$ ,  $A\beta(34-40)$ , and  $A\beta(21-30)$  showed nonfibrillar aggregates. The morphology of  $A\beta(35-42)$  is shown as an example in

Figure 3.  $A\beta(34-42)$  and longer  $A\beta 42$  CTFs, except  $A\beta(32-42)$ , were found to form fibrils, which displayed substantial morphological variability. On day 1,  $A\beta(34-42)$  formed long ( $> 500$  nm) fibrils with diameter  $d = 17 \pm 1$  nm. After 7 days, wide, ribbon-like fibrils with diameter  $26 \pm 2$  nm were observed. Fibrils of  $A\beta(31-42)$  and  $A\beta(33-42)$  had a twisted, filamentous morphology. The average diameters of  $A\beta(31-42)$  and  $A\beta(33-42)$  fibrils were  $5.0 \pm 0.2$  and  $10.2 \pm 0.9$  nm on day 1, respectively, and they were  $> 500$  nm long. The morphology of these fibrils did not change appreciably between day 1 and day 7.

$A\beta(28-42)$ ,  $A\beta(29-42)$ , and  $A\beta(30-42)$  were examined at concentrations  $\leq 10 \mu\text{M}$ . On day 1, nonfibrillar aggregates or short threads were observed, whereas on day 7, the morphology was characterized by multiple short fibrils (average diameter =  $8.8 \pm 0.5$  nm, average length =  $72 \pm 6$  nm). The appearance of multiple short fibrils is in agreement with formation of multiple nuclei, consistent with fast aggregation and  $\beta$ -sheet formation of these peptides. In contrast, the shorter peptides,  $A\beta(31-42)$  through  $A\beta(34-42)$ , except  $A\beta(32-42)$ , yielded long fibrils, suggesting that for these peptides the rate of fibril elongation was substantially higher than the rate of nucleation.

Immediately after preparation, thread-like structures were observed for  $A\beta(32-42)$ , whereas at day 7, the predominant morphology was nonfibrillar aggregates as predicted for this CTF based on the combination of relatively low solubility, slow aggregation, and no observation of  $\beta$ -sheet formation.  $A\beta(30-40)$  showed predominantly nonfibrillar aggregates on day 1, whereas on day 7, long ( $> 500$  nm) and twisted fibrils,  $12 \pm 1$  nm in diameter, were observed.

## DISCUSSION

Previously,  $A\beta 42$  CTFs were found to inhibit the neurotoxicity inflicted by full-length  $A\beta 42$ , supporting the idea that peptides derived from the C-terminus of  $A\beta 42$  would disrupt the assembly of  $A\beta 42$  into toxic oligomers. Here, we expanded our initial study (20) to a systematic biophysical characterization of solubility and aggregation of all the CTFs reported previously and included two  $A\beta 40$  CTFs and the fragment  $A\beta(21-30)$  derived from the putative  $A\beta$  folding nucleus.

As shown in Table 1, using a filtration method to estimate peptide solubility, we found that  $A\beta(33-42)$  and shorter peptides

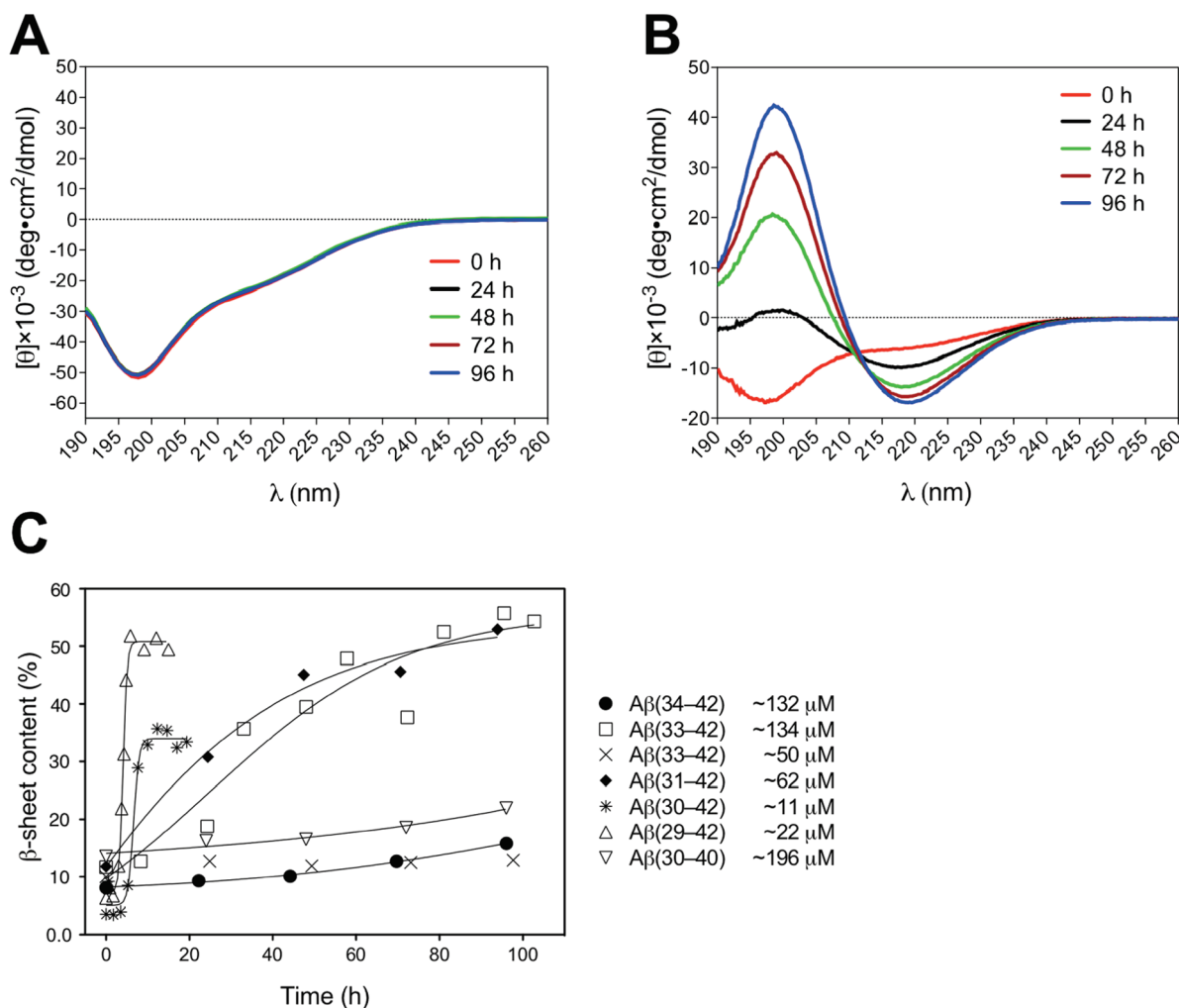


FIGURE 2: Time-dependent conformational change. (A) Representative CD spectra of 156  $\mu\text{M}$  A $\beta$ (38–42) recorded in time intervals of 24 h. The spectra showing a minimum at 197 nm are characteristic of a statistical coil and remain unchanged for 4 days. (B) Representative CD spectra of 62  $\mu\text{M}$  A $\beta$ (31–42) recorded in time intervals of 24 h. The initial spectrum showing a minimum at 197 nm is characteristic of a statistical coil. The development of a maximum at 198 nm and a minimum at 218 nm indicates conformational change to  $\beta$ -sheet-rich structures. (C) Representative time course of  $\beta$ -sheet formation calculated as described in Materials and Methods is shown for A $\beta$ (29–42), A $\beta$ (30–42), A $\beta$ (31–42), A $\beta$ (33–42), A $\beta$ (34–42), and A $\beta$ (30–40) at the concentrations indicated.

were soluble at  $>100 \mu\text{M}$ , whereas longer peptides had substantially lower solubility. The data indicate that CTF solubility relates roughly to peptide length and depends on the particular amino acid sequence of each peptide. The inclusion of the two A $\beta$ 40 CTFs in the current study revealed that the presence of the C-terminal dipeptide, I41-A42, confers a strong decrease in solubility (cf. A $\beta$ (30–40) with A $\beta$ (30–42) and A $\beta$ (34–40) with A $\beta$ (34–42), Table 1), supporting the idea that these two residues stabilize aggregation-prone conformations in A $\beta$ ( $x$ –42) relative to A $\beta$ ( $x$ –40).

A $\beta$ (34–42) has been studied previously by solid-state NMR and found to form fibrils in which the peptide chains were in an antiparallel arrangement (38). Here, we asked if fibril formation was a common phenomenon to all CTFs or whether the low solubility we observed for CTFs longer than A $\beta$ (35–42) might have reflected amorphous aggregation. Peptide/protein fibrillation depends on a number of factors, including hydrophathy (39), secondary structure propensity of each residue (40), the context of each residue within the sequence (41–43), and peptide length. Comparison of solubility, rates of particle growth (DLS) and conformational transition (CD), and morphology (EM) was difficult because not all peptides could be dissolved at the same

concentration. One way to overcome this difficulty would have been by comparing all of the peptides at the maximal concentration of the least soluble CTF. However, this would have resulted in low signal-to-noise ratio in DLS and CD experiments and likely would have required very long measurement times to observe aggregation of certain CTFs. Instead, we chose to study each CTF near its highest concentration as determined by the filtration assay described above and, in particular cases, to compare certain CTFs at higher dilutions.

We found that A $\beta$ (35–42) and shorter CTFs did not aggregate, convert to  $\beta$ -sheet, or form fibrils within the time frame of measurement at concentrations  $>100 \mu\text{M}$ . In contrast, A $\beta$ (34–42) and longer CTFs, except A $\beta$ (32–42), aggregated into  $\beta$ -sheet-rich fibrils (Table 1 and Figures 1–3).

However, despite this simple division of the CTF series to short (4–8 residues) and long (9–15 residues), analysis of the different data sets showed that the relations among peptide length, solubility, fibrillogenesis tendency, and inhibitory activity were complex. For example, in some cases, peptides with similar lengths behaved similarly but, in other cases, differed substantially. Thus, taking into account the differences in concentration, A $\beta$ (29–42) and A $\beta$ (30–42) or A $\beta$ (31–42) and A $\beta$ (33–42) had

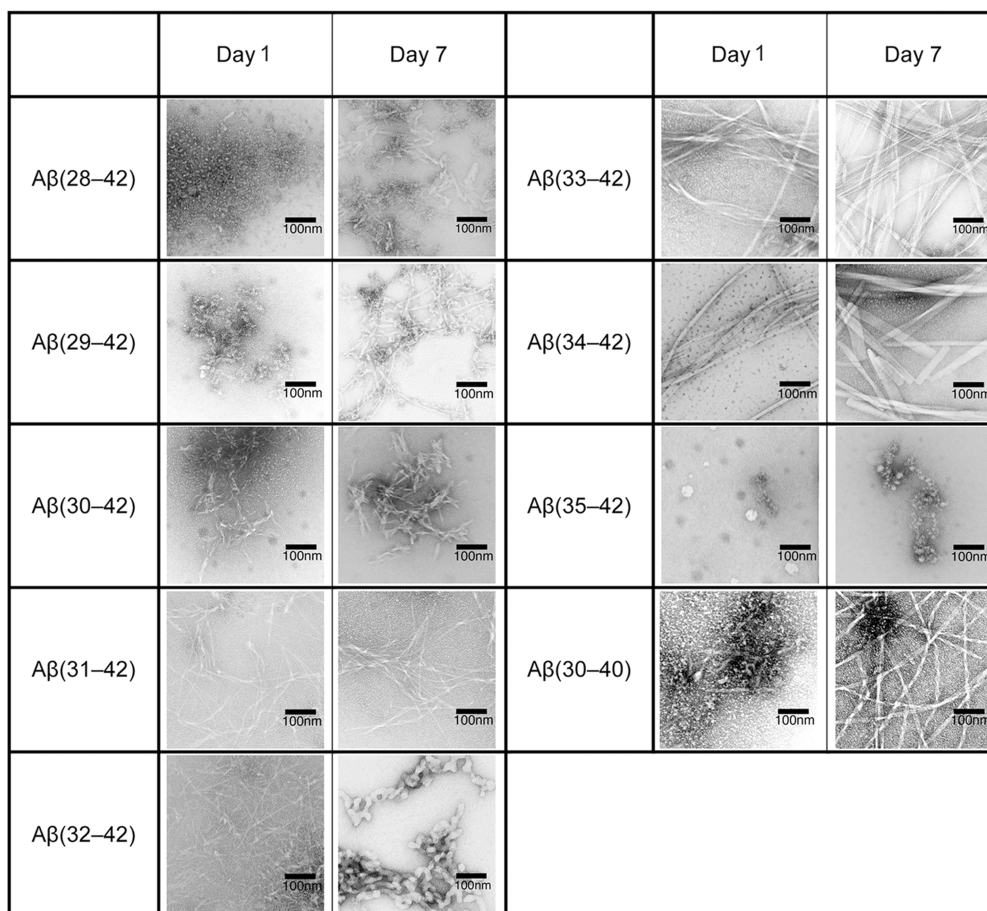


FIGURE 3: Time-dependent peptide morphology. Peptide solutions used were of the following concentrations:  $A\beta(28-42)$ ,  $1 \pm 0.7 \mu\text{M}$ ;  $A\beta(29-42)$ ,  $14 \pm 1 \mu\text{M}$ ;  $A\beta(30-42)$ ,  $9 \pm 0.5 \mu\text{M}$ ;  $A\beta(31-42)$ ,  $22 \pm 0.6 \mu\text{M}$ ;  $A\beta(32-42)$ ,  $16 \pm 0.6 \mu\text{M}$ ;  $A\beta(33-42)$ ,  $80.0 \pm 0.1 \mu\text{M}$ ;  $A\beta(34-42)$ ,  $99 \pm 4 \mu\text{M}$ ;  $A\beta(35-42)$ ,  $122 \pm 1 \mu\text{M}$ ;  $A\beta(30-40)$ ,  $191 \pm 10 \mu\text{M}$ . Electron micrographs were recorded immediately after sample preparation (day 1) and 1 week later (day 7).

comparable aggregation rates, whereas the aggregation rates of  $A\beta(30-42)$  and  $A\beta(31-42)$  differed substantially (Figure 1B). These data suggest that above the 8-residue cutoff, under which little or no aggregation is detected, aggregation rate and fibril formation depend on the particular amino acid sequence of each peptide and the context of each residue.

To gain a better understanding of how solubility and aggregation tendency correlate with each other and with the biological activity of the peptides, we calculated linear correlations among the different data sets, which, depending on the parameter, ranged from as little as 3 to as many as 15 data points for the entire peptide series. This analysis showed that solubility alone was a poor predictor of the aggregation tendency or biological activity of peptides. The  $r^2$  values calculated for the correlation of peptide solubility with rate of aggregation ( $dR_H/dt$ , DLS measurement), half-maximal time of  $\beta$ -sheet formation ( $T_{50}$ , CD measurement), or inhibitory activity ( $IC_{50}$ , MTT assay) were 0.42, 0.41 (not shown), and 0.04 (Figure 4A), respectively. In contrast, as might be expected, the rates of aggregation and  $\beta$ -sheet formation were correlated ( $r^2 = 0.86$ , Figure 4B). However, neither of these parameters showed high correlation with inhibition of  $A\beta(42)$ -induced toxicity ( $IC_{50}$  with  $dR_H/dt$ ,  $r^2 = 0.45$ ;  $IC_{50}$  with  $T_{50}$ ,  $r^2 = 0.30$ , not shown).

Next, we asked whether a correlation existed between any of the physical parameters measured here or the inhibition of  $A\beta(42)$ -induced toxicity and the three-dimensional structures of the CTFs. Recently, Wu et al. have used ion-mobility mass

spectrometry (IM-MS) combined with all-atom molecular dynamics (MD) simulations in the gas phase to examine the conformation of  $A\beta$  CTFs. In addition, the conformation of several CTFs was further calculated in the presence of explicit water molecules. Two predominant aqueous conformations were found:  $\beta$ -hairpin and “coil–turn” (44).  $A\beta(29-42)$  and  $A\beta(30-42)$  were reported to have a similar propensity ( $\sim 40\%$ ) to form  $\beta$ -hairpin, whereas shortening the sequence by one N-terminal residue to  $A\beta(31-42)$  reduced the  $\beta$ -hairpin propensity to  $\sim 25\%$ . Removal of the two C-terminal residues of  $A\beta(30-42)$  resulted in a dramatic decrease of  $\beta$ -hairpin formation propensity from 40% to 4% in  $A\beta(30-40)$ . In agreement with their lower tendency to form a  $\beta$ -hairpin,  $A\beta(31-42)$  and  $A\beta(30-40)$  showed higher tendency to form a coil–turn structure (29% and 28%, respectively) than  $A\beta(30-42)$  (16%) and  $A\beta(29-42)$  (4%) (Table 1).

The  $\beta$ -hairpin propensities reported by Wu et al. showed moderate to high correlation with the CTFs' solubility ( $r^2 = 0.95$ ), aggregation rate  $dR_H/dt$  ( $r^2 = 0.78$ ), and  $T_{50}$  of  $\beta$ -sheet formation ( $r^2 = 0.99$ ) (Figures 4C–E). Interestingly,  $IC_{50}$  values of inhibition of  $A\beta(42)$ -induced toxicity showed relatively high correlation with coil–turn conformation propensity of CTFs ( $r^2 = 0.85$ ) (Figure 4F). Taken together, the data suggest that of the longer CTFs studied here those that tend to adopt a  $\beta$ -hairpin conformation, such as  $A\beta(29-42)$  and  $A\beta(30-42)$ , have low solubility, form abundant fibrillogenesis nuclei, and aggregate rapidly into short  $\beta$ -sheet-rich fibrils. In contrast, CTFs that have

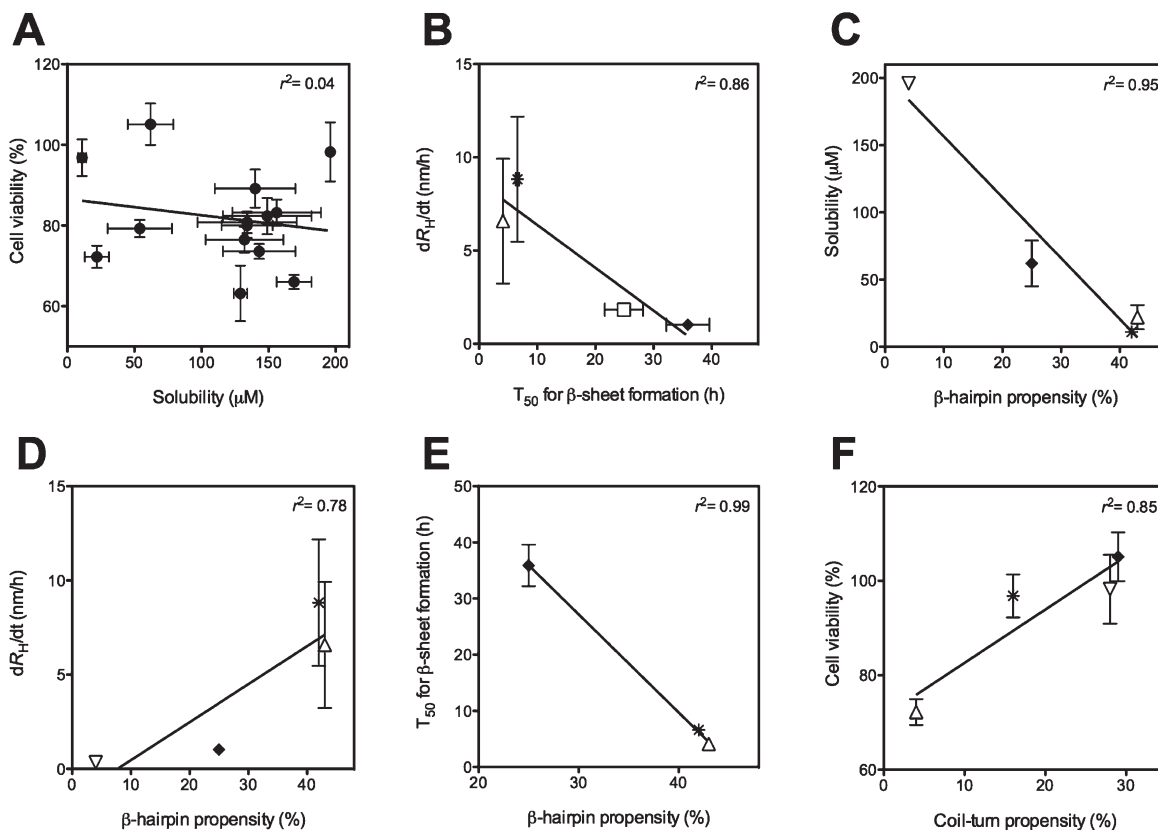


FIGURE 4: Relationships among biophysical and biological properties. (A) Linear regression analysis correlating inhibition of A $\beta$ 42-induced toxicity with CTF solubility ( $r^2 = 0.04$ ,  $p = 0.52$ ). (B) Linear regression analysis correlating aggregation rates of A $\beta$ (29–42), A $\beta$ (30–42), A $\beta$ (31–42), and A $\beta$ (33–42) with  $T_{50}$  values of  $\beta$ -sheet formation ( $r^2 = 0.86$ ,  $p = 0.07$ ). (C) Linear regression analysis correlating solubility of A $\beta$ (29–42), A $\beta$ (30–42), A $\beta$ (31–42), and A $\beta$ (30–40) with propensity for  $\beta$ -hairpin conformation ( $r^2 = 0.95$ ,  $p = 0.03$ ). (D) Linear regression analysis correlating aggregation rates of A $\beta$ (29–42), A $\beta$ (30–42), A $\beta$ (31–42), and A $\beta$ (30–40) with propensity for  $\beta$ -hairpin conformation ( $r^2 = 0.78$ ,  $p = 0.11$ ). (E) Linear regression analysis correlating  $T_{50}$  values of  $\beta$ -sheet formation of A $\beta$ (29–42), A $\beta$ (30–42), and A $\beta$ (31–42) with propensity for  $\beta$ -hairpin conformation ( $r^2 = 0.99$ ,  $p = 0.01$ ). (F) Linear regression analysis correlating inhibition of A $\beta$ 42-induced toxicity of A $\beta$ (29–42), A $\beta$ (30–42), A $\beta$ (31–42), and A $\beta$ (30–40) with propensity for coil–turn conformation ( $r^2 = 0.85$ ,  $p = 0.08$ ). The symbols used in panels B–F are  $\triangle$  for A $\beta$ (29–42), \* for A $\beta$ (30–42),  $\blacklozenge$  for A $\beta$ (31–42),  $\square$  for A $\beta$ (33–42), and  $\nabla$  for A $\beta$ (30–40).

a relatively low tendency to form  $\beta$ -hairpin, such as A $\beta$ (31–42) and A $\beta$ (30–40), have higher solubility, form few nuclei, and aggregate at slower rates into long fibrils. The latter three peptides, A $\beta$ (30–42), A $\beta$ (31–42), and A $\beta$ (30–40), are strong inhibitors of A $\beta$ 42-induced toxicity, presumably thanks to interaction with full-length A $\beta$ 42 enabled by their coil–turn conformation (Figure 4F).

The contextual importance of position of each amino acid residue in the sequence is highlighted by comparing A $\beta$ (32–42) with A $\beta$ (30–40). Both of these peptides comprise 11 residues, and they share >80% sequence identity. Moreover, the two N-terminal residues of A $\beta$ (30–40), A30 and I31, are identical, in reverse order, to the C-terminal I41 and A42 in A $\beta$ (32–42). Nevertheless, A $\beta$ (30–40) formed  $\beta$ -sheet-rich fibrils whereas A $\beta$ (32–42) did not. Surprisingly, despite this behavior, A $\beta$ (30–40) was  $\sim$ 4 times more soluble than A $\beta$ (32–42). In addition, in contrast to the poor inhibitory activity and slight toxicity of A $\beta$ (32–42) (20), A $\beta$ (30–40) was a strong inhibitor of A $\beta$ 42 toxicity.

The longest CTF included in our study, A $\beta$ (28–42), stood apart from the rest of the peptides. A $\beta$ (28–42) had the lowest solubility of all CTFs and was the only sequence displaying higher toxicity than A $\beta$ 42 itself (20). One explanation for the low solubility observed is the amphipathic nature of the K side chain, which includes a long hydrophobic butylene arm and a positively charged amino group. Though K typically is

considered a hydrophilic residue, hydrophobic interactions of the butylene moiety with other side chains (45) may explain the considerable decrease in solubility of A $\beta$ (28–42) relative to A $\beta$ (29–42).

The high toxicity of A $\beta$ (28–42) may be explained, at least partially, by Coulomb interactions between the positive charge of K28 in A $\beta$ (28–42) and negatively charged phosphate head-groups of membrane phospholipids. Similar to A $\beta$ (28–42), A $\beta$ (25–35) has a net +1 charge and is highly toxic (46). In both A $\beta$ (28–42) and A $\beta$ (25–35), the net positive charge results from the  $\epsilon$ -NH $_3^+$  group of K28, which also has been proposed to mediate the interaction of full-length A $\beta$  with the plasma membrane (47). Interestingly, most of the amino acid substitutions in A $\beta$  that cause familial AD and/or cerebral amyloid angiopathy, namely, those caused by the Dutch (E22Q) (48), Arctic (E22G) (49), Iowa (D23N) (50), Tottori (D7N) (51), and English (H6R) (52) mutations, and the recently discovered deletion of glutamate 22 (E22 $\Delta$ ) (53, 54), cause an increase of one unit in the positive charge of A $\beta$ . The Italian mutation (E22K) (55) causes an increase of two positive charge units. Thus, increased positive charge may be an important factor contributing to the toxic effect of amyloidogenic/hydrophobic peptides, presumably by increasing their tendency to interact with negatively charged membranes.

In summary, our study suggests that although grossly the biophysical properties of A $\beta$ 42 CTFs are length-dependent, the

correlation between peptide length, peptide conformation, solubility, aggregation tendency, and inhibitory activity is complex. Peptides up to 8 residues long have relatively high solubility and low aggregation propensity. Longer peptides have low aqueous solubility and, excluding A $\beta$ (32–42), readily form  $\beta$ -sheet-rich fibrils. The presence of the C-terminal dipeptide, I41-A42, increases these tendencies substantially. Aggregation rates of CTFs correlate with  $\beta$ -hairpin propensity and  $\beta$ -sheet formation. In contrast, inhibition of A $\beta$ 42-induced toxicity shows poor correlation with peptide length, solubility, aggregation rate,  $\beta$ -hairpin propensity in the monomer, or  $\beta$ -sheet formation in the fibril but correlates with a propensity to form a coil–turn conformation. These results shed light on the parameters that modulate the biophysical properties and the inhibitory activity of the CTFs. The data provide guidelines for design of future generations of CTF-based inhibitors with improved characteristics against A $\beta$ -induced toxicity.

## ACKNOWLEDGMENT

We thank Dr. David Teplow for use of his DLS and CD spectrometers and Drs. Farid Rahimi, Sharmistha Sinha, and Panchanan Maiti for helpful discussions.

## REFERENCES

- Walsh, D. M., and Selkoe, D. J. (2007) A $\beta$  oligomers—a decade of discovery. *J. Neurochem.* *101*, 1172–1184.
- Kirkpatrick, M. D., Bitan, G., and Teplow, D. B. (2002) Paradigm shifts in Alzheimer's disease and other neurodegenerative disorders: the emerging role of oligomeric assemblies. *J. Neurosci. Res.* *69*, 567–577.
- Hardy, J., and Selkoe, D. J. (2002) The amyloid hypothesis of Alzheimer's disease: progress and problems on the road to therapeutics. *Science* *297*, 353–356.
- Ferreira, S. T., Vieira, M. N., and De Felice, F. G. (2007) Soluble protein oligomers as emerging toxins in Alzheimer's and other amyloid diseases. *IUBMB Life* *59*, 332–345.
- Lesné, S., Koh, M. T., Kotilinek, L., Kaye, R., Glabe, C. G., Yang, A., Gallagher, M., and Ashe, K. H. (2006) A specific amyloid- $\beta$  protein assembly in the brain impairs memory. *Nature* *440*, 352–357.
- Shankar, G. M., Li, S., Mehta, T. H., Garcia-Munoz, A., Shepardson, N. E., Smith, I., Brett, F. M., Farrell, M. A., Rowan, M. J., Lemere, C. A., Regan, C. M., Walsh, D. M., Sabatini, B. L., and Selkoe, D. J. (2008) Amyloid- $\beta$  protein dimers isolated directly from Alzheimer's brains impair synaptic plasticity and memory. *Nat. Med.* *14*, 837–842.
- Dahlgren, K. N., Manelli, A. M., Stine, W. B., Jr., Baker, L. K., Krafft, G. A., and LaDu, M. J. (2002) Oligomeric and fibrillar species of amyloid- $\beta$  peptides differentially affect neuronal viability. *J. Biol. Chem.* *277*, 32046–32053.
- Bitan, G., Kirkpatrick, M. D., Lomakin, A., Vollers, S. S., Benedek, G. B., and Teplow, D. B. (2003) Amyloid  $\beta$ -protein (A $\beta$ ) assembly: A $\beta$ 40 and A $\beta$ 42 oligomerize through distinct pathways. *Proc. Natl. Acad. Sci. U.S.A.* *100*, 330–335.
- Chen, Y.-R., and Glabe, C. G. (2006) Distinct early folding and aggregation properties of Alzheimer amyloid- $\beta$  peptides A $\beta$ 40 and A $\beta$ 42: stable trimer or tetramer formation by A $\beta$ 42. *J. Biol. Chem.* *281*, 24414–24422.
- Bitan, G., Vollers, S. S., and Teplow, D. B. (2003) Elucidation of primary structure elements controlling early amyloid  $\beta$ -protein oligomerization. *J. Biol. Chem.* *278*, 34882–34889.
- Lazo, N. D., Grant, M. A., Condrón, M. C., Rigby, A. C., and Teplow, D. B. (2005) On the nucleation of amyloid  $\beta$ -protein monomer folding. *Protein Sci.* *14*, 1581–1596.
- Urbanc, B., Cruz, L., Yun, S., Buldyrev, S. V., Bitan, G., Teplow, D. B., and Stanley, H. E. (2004) *In silico* study of amyloid  $\beta$ -protein folding and oligomerization. *Proc. Natl. Acad. Sci. U.S.A.* *101*, 17345–17350.
- Yun, S., Urbanc, B., Cruz, L., Bitan, G., Teplow, D. B., and Stanley, H. E. (2007) Role of electrostatic interactions in amyloid  $\beta$ -protein (A $\beta$ ) oligomer formation: a discrete molecular dynamics study. *Biophys. J.* *92*, 4064–4077.
- Yang, M., and Teplow, D. B. (2008) Amyloid  $\beta$ -protein monomer folding: free-energy surfaces reveal alloform-specific differences. *J. Mol. Biol.* *384*, 450–464.
- Riek, R., Guntert, P., Dobeli, H., Wipf, B., and Wüthrich, K. (2001) NMR studies in aqueous solution fail to identify significant conformational differences between the monomeric forms of two Alzheimer peptides with widely different plaque-competence, A $\beta$ (1–40)(ox) and A $\beta$ (1–42)(ox). *Eur. J. Biochem.* *268*, 5930–5936.
- Hou, L., Shao, H., Zhang, Y., Li, H., Menon, N. K., Neuhaus, E. B., Brewer, J. M., Byeon, I. J., Ray, D. G., Vitek, M. P., Iwashita, T., Makula, R. A., Przybyla, A. B., and Zagorski, M. G. (2004) Solution NMR studies of the A $\beta$ (1–40) and A $\beta$ (1–42) peptides establish that the Met35 oxidation state affects the mechanism of amyloid formation. *J. Am. Chem. Soc.* *126*, 1992–2005.
- Sgourakis, N. G., Yan, Y., McCallum, S. A., Wang, C., and Garcia, A. E. (2007) The Alzheimer's peptides A $\beta$ 40 and 42 adopt distinct conformations in water: a combined MD/NMR study. *J. Mol. Biol.* *368*, 1448–1457.
- Yan, Y., and Wang, C. (2006) A $\beta$ 42 is more rigid than A $\beta$ 40 at the C terminus: implications for A $\beta$  aggregation and toxicity. *J. Mol. Biol.* *364*, 853–862.
- Condrón, M. M., Monien, B. H., and Bitan, G. (2008) Synthesis and purification of highly hydrophobic peptides derived from the C-terminus of amyloid  $\beta$ -protein. *Open Biotechnol. J.* *2*, 87–93.
- Fradinger, E. A., Monien, B. H., Urbanc, B., Lomakin, A., Tan, M., Li, H., Spring, S. M., Condrón, M. M., Cruz, L., Xie, C. W., Benedek, G. B., and Bitan, G. (2008) C-terminal peptides coassemble into A $\beta$ 42 oligomers and protect neurons against A $\beta$ 42-induced neurotoxicity. *Proc. Natl. Acad. Sci. U.S.A.* *105*, 14175–14180.
- Merrifield, R. B. (1965) Automated synthesis of peptides. *Science* *150*, 178–185.
- Lomakin, A., Chung, D. S., Benedek, G. B., Kirschner, D. A., and Teplow, D. B. (1996) On the nucleation and growth of amyloid  $\beta$ -protein fibrils: detection of nuclei and quantitation of rate constants. *Proc. Natl. Acad. Sci. U.S.A.* *93*, 1125–1129.
- Tikhonov, A. N., and Arsenin, V. Y. (1977) *Solution of Ill-Posed Problems*, Halsted Press, Washington, DC.
- Sreerama, N., and Woody, R. W. (1993) A self-consistent method for the analysis of protein secondary structure from circular dichroism. *Anal. Biochem.* *209*, 32–44.
- Provencher, S. W., and Glockner, J. (1981) Estimation of globular protein secondary structure from circular dichroism. *Biochemistry* *20*, 33–37.
- Johnson, W. C. (1999) Analyzing protein circular dichroism spectra for accurate secondary structures. *Proteins* *35*, 307–312.
- Abe, K., and Saito, H. (1998) Amyloid  $\beta$  protein inhibits cellular MTT reduction not by suppression of mitochondrial succinate dehydrogenase but by acceleration of MTT formazan exocytosis in cultured rat cortical astrocytes. *Neurosci. Res.* *31*, 295–305.
- Datki, Z., Juhasz, A., Galfi, M., Soos, K., Papp, R., Zadori, D., and Penke, B. (2003) Method for measuring neurotoxicity of aggregating polypeptides with the MTT assay on differentiated neuroblastoma cells. *Brain Res. Bull.* *62*, 223–229.
- Shearman, M. S., Ragan, C. I., and Iversen, L. L. (1994) Inhibition of PC12 cell redox activity is a specific, early indicator of the mechanism of  $\beta$ -amyloid-mediated cell death. *Proc. Natl. Acad. Sci. U.S.A.* *91*, 1470–1474.
- Pereira, C., Santos, M. S., and Oliveira, C. (1998) Mitochondrial function impairment induced by amyloid  $\beta$ -peptide on PC12 cells. *Neuroreport* *9*, 1749–1755.
- Grant, M. A., Lazo, N. D., Lomakin, A., Condrón, M. M., Arai, H., Yamin, G., Rigby, A. C., and Teplow, D. B. (2007) Familial Alzheimer's disease mutations alter the stability of the amyloid  $\beta$ -protein monomer folding nucleus. *Proc. Natl. Acad. Sci. U.S.A.* *104*, 16522–16527.
- Fawzi, N. L., Phillips, A. H., Ruscio, J. Z., Doucleff, M., Wemmer, D. E., and Head-Gordon, T. (2008) Structure and dynamics of the A $\beta$ (21–30) peptide from the interplay of NMR experiments and molecular simulations. *J. Am. Chem. Soc.* *130*, 6145–6158.
- Serpell, L. C. (2000) Alzheimer's amyloid fibrils: structure and assembly. *Biochim. Biophys. Acta* *1502*, 16–30.
- Li, H., Rahimi, F., Murakami, K., Sinha, S., Maiti, P., and Bitan, G. (2009) Amyloids and protein aggregation—analytical methods, in *Encyclopedia of Analytical Chemistry* (Meyers, R. A., Ed.) John Wiley & Sons, New York.
- Lomakin, A., Teplow, D. B., Kirschner, D. A., and Benedek, G. B. (1997) Kinetic theory of fibrillogenesis of amyloid  $\beta$ -protein. *Proc. Natl. Acad. Sci. U.S.A.* *94*, 7942–7947.

36. Lomakin, A., Benedek, G. B., and Teplow, D. B. (1999) Monitoring protein assembly using quasielastic light scattering spectroscopy. *Methods Enzymol.* 309, 429–459.
37. Lomakin, A., Teplow, D. B., and Benedek, G. B. (2005) Quasielastic light scattering for protein assembly studies. *Methods Mol. Biol.* 299, 153–174.
38. Lansbury, P. T., Jr., Costa, P. R., Griffiths, J. M., Simon, E. J., Auger, M., Halverson, K. J., Kocisko, D. A., Hendsch, Z. S., Ashburn, T. T., and Spencer, R. G.; et al. (1995) Structural model for the  $\beta$ -amyloid fibril based on interstrand alignment of an antiparallel-sheet comprising a C-terminal peptide. *Nat. Struct. Biol.* 2, 990–998.
39. Kyte, J., and Doolittle, R. F. (1982) A simple method for displaying the hydropathic character of a protein. *J. Mol. Biol.* 157, 105–132.
40. Chou, P. Y., and Fasman, G. D. (1974) Conformational parameters for amino acids in helical,  $\beta$ -sheet, and random coil regions calculated from proteins. *Biochemistry* 13, 211–222.
41. Bellesia, G., and Shea, J. E. (2009) Effect of  $\beta$ -sheet propensity on peptide aggregation. *J. Chem. Phys.* 130, 145103.
42. Chiti, F., Stefani, M., Taddei, N., Ramponi, G., and Dobson, C. M. (2003) Rationalization of the effects of mutations on peptide and protein aggregation rates. *Nature* 424, 805–808.
43. DuBay, K. F., Pawar, A. P., Chiti, F., Zurdo, J., Dobson, C. M., and Vendruscolo, M. (2004) Prediction of the absolute aggregation rates of amyloidogenic polypeptide chains. *J. Mol. Biol.* 341, 1317–1326.
44. Wu, C., Murray, M. M., Bernstein, S. L., Condrón, M. M., Bitan, G., Shea, J. E., and Bowers, M. T. (2009) The structure of A $\beta$ 42 C-terminal fragments probed by a combined experimental and theoretical study. *J. Mol. Biol.* 387, 492–501.
45. Petsko, G. A., and Ringe, D. (2004) Protein Structure and Function, New Science Press, Sunderland, MA.
46. Dante, S., Hauss, T., and Dencher, N. A. (2002)  $\beta$ -amyloid 25 to 35 is intercalated in anionic and zwitterionic lipid membranes to different extents. *Biophys. J.* 83, 2610–2616.
47. Chauhan, A., Ray, I., and Chauhan, V. P. (2000) Interaction of amyloid  $\beta$ -protein with anionic phospholipids: possible involvement of Lys28 and C-terminus aliphatic amino acids. *Neurochem. Res.* 25, 423–429.
48. Levy, E., Carman, M. D., Fernandez-Madrid, I. J., Power, M. D., Lieberburg, I., van Duinen, S. G., Bots, G. T., Luyendijk, W., and Frangione, B. (1990) Mutation of the Alzheimer's disease amyloid gene in hereditary cerebral hemorrhage, Dutch type. *Science* 248, 1124–1126.
49. Nilsberth, C., Westlind-Danielsson, A., Eckman, C. B., Condrón, M. M., Axelman, K., Forsell, C., Sten, C., Luthman, J., Teplow, D. B., Younkin, S. G., Naslund, J., and Lannfelt, L. (2001) The "Arctic" APP mutation (E693G) causes Alzheimer's disease by enhanced A $\beta$  protofibril formation. *Nat. Neurosci.* 4, 887–893.
50. Van Nostrand, W. E., Melchor, J. P., Cho, H. S., Greenberg, S. M., and Rebeck, G. W. (2001) Pathogenic effects of D23N Iowa mutant amyloid  $\beta$ -protein. *J. Biol. Chem.* 276, 32860–32866.
51. Wakutani, Y., Watanabe, K., Adachi, Y., Wada-Isoe, K., Urakami, K., Ninomiya, H., Saido, T. C., Hashimoto, T., Iwatsubo, T., and Nakashima, K. (2004) Novel amyloid precursor protein gene missense mutation (D678N) in probable familial Alzheimer's disease. *J. Neurol., Neurosurg. Psychiatry* 75, 1039–1042.
52. Janssen, J. C., Beck, J. A., Campbell, T. A., Dickinson, A., Fox, N. C., Harvey, R. J., Houlden, H., Rossor, M. N., and Collinge, J. (2003) Early onset familial Alzheimer's disease: mutation frequency in 31 families. *Neurology* 60, 235–239.
53. Tomiyama, T., Nagata, T., Shimada, H., Teraoka, R., Fukushima, A., Kanemitsu, H., Takuma, H., Kuwano, R., Imagawa, M., Ataka, S., Wada, Y., Yoshioka, E., Nishizaki, T., Watanabe, Y., and Mori, H. (2008) A new amyloid  $\beta$  variant favoring oligomerization in Alzheimer's-type dementia. *Ann. Neurol.* 63, 377–387.
54. Takuma, H., Teraoka, R., Mori, H., and Tomiyama, T. (2008) Amyloid- $\beta$  E22 $\Delta$  variant induces synaptic alteration in mouse hippocampal slices. *Neuroreport* 19, 615–619.
55. Miravalle, L., Tokuda, T., Chiarle, R., Giaccone, G., Bugiani, O., Tagliavini, F., Frangione, B., and Ghiso, J. (2000) Substitutions at codon 22 of Alzheimer's A $\beta$  peptide induce diverse conformational changes and apoptotic effects in human cerebral endothelial cells. *J. Biol. Chem.* 275, 27110–27116.